2021 20th IEEE Intersociety Conference on Thermal and Thermomechanical Phenomena in Electronic Systems (iTherm) | 978-1-7281-8539-2/21/$31.00 ©2021 IEEE | DOI: 10.1109/ITherm51669.2021.9503283

Two-phase Impingement Cooling using a Trapezoidal Groove Microchannel Heat Sink and Dielectric Coolant HFE 7000

[a]Cong Hiep Hoang, [a]Srikanth Rangarajan, [a]Vahideh Radmard, [a]Najmeh Fallahtafti, [a]Mohammad Tradat, [b]Charles Arvin, [a]Scott Schiffres, [a]Bahgat Sammakia

[a]Department of Mechanical Engineering, State University of New York at Binghamton, Binghamton, NY, USA
[b]IBM Corporation, NY, USA

***Abstract*— This paper focuses on two-phase flow boiling of dielectric coolant HFE 7000 inside a copper multi-microchannel heat sink for high heat flux chip applications. The heat sink is composed of parallel microchannels, 200 µm wide, 2500 µm high, and 20 mm long, with 200-µm-thick fins separating the channels. The copper heat sink consists of almost 100 channels connected by a longitude groove with a nearly trapezoidal cross section. Coolant impinges down to the base at the groove and then goes along the microchannels. A copper block heater arrangement was used to mimic a computer chip with a footprint of 1"x1" (6.45 cm^2). The base heat flux was varied from 7.75 W/cm^2 to 96.1 W/cm^2 and the mass flux from 547.6 to 958.4 kg/m^{2}s, at a nominal saturation temperature of 54 °C. Heat transfer coefficients as high as 57.5 kW/m^{2}K were reached, keeping the base temperature under 66 ° C with a maximum of 21.9 kPa of pressure drop, for inlet subcooling of 5 degree and a coolant flow rate of 958.4 kg/m^2. Effects of inner diameter of tubing on thermal performance and pressure drop are also discussed. It was observed that an increase of tubing inner diameter by 60 % can result in increase of heat transfer coefficient by 47.8 % and reduction in pressure drop by 63 %.**

Keywords. Two-phase cooling, boiling, microchannel, Impingement.

Nomenclature.

R_{th}	specific thermal resistance (Kcm^2/W)
T_b	base temperature of the heat sink (°C)
T_i	coolant inlet temperature (°C)
T_{out}	coolant outlet temperature (°C)
ΔP	pressure drop (kPa)

1. Introduction

Electronics cooling is a growing concern in industry and government organizations. Global data centers consumed around 200 billion kWh/year [1] corresponding to 1.3 % of global electricity use and cooling was reported to consume roughly 33 % of total energy used in legacy data centers [2]. It was predicted that the United States data center energy consumption increase by 4% from 2014-2020 and reach 73 billion kWh in 2020 [3]. Increasing power densities due to the rise of Artificial Intelligence (AI), high-performance computing (HPC) and machine learning can lead to the increasing cost and complexity of thermal management in electronics device. State of art heat flux in electronics cooling already exceeded the capability of air-cooling technology. Owing to high specific heat and latent heat of liquid coolants, liquid cooling is an alternative solution. An IBM study [4] showed that cooling efficiency with liquid cooling can be 3500 times higher than air cooling. Single-phase cooling with water is currently the most popular liquid cooling method in data center and shows high heat transfer coefficient and acceptable pumping power [5-10]. It is reported in [11,12] that the highest heat transfer rate of single-phase cooling cold plate with water can be up to 1150W. Although having high thermal performance, single-phase cooling also has disadvantages such as high temperature gradient along chip surface and dangerous consequences of a fluid leak. By combining a non-conductive dielectric refrigerant with boiling heat transfer, pumped two-phase cooling products can increase power densities for high power electronics by more than 2x over traditional water / glycol systems [11,13], while eliminating the dangerous consequences of a fluid leak. Two-phase cooling not only surpasses the basic cooling configurations in heat dissipation rate, but it also provides better surface temperature uniformity due to the evaporation of coolant at saturation temperature.

There are many research studies in literature focused on the component level where effects of operating parameters and geometry parameters on thermal and hydraulic performance of cold plate are quantified. Three cooling strategies were studied in [14]: copper cold-plate micro-channel module bonded to the device substrate, embedded micro-channels directly etched into the device substrate and, embedded micro-channels with a 3D manifold with inlet and outlet module. The embedded micro-channels with 3D-manifold with R245fa working fluid has the potential to achieve the lowest thermal resistance. Three types of micro pin fins (triangular, hexagonal, and circular) cold plates were fabricated by silicon processes [15]. The triangular micro pin fins could promote the flow and mixing of the coolant to eliminate the slug flow and therefore; had the best heat transfer characteristics and pressure drop performance. A potential stacked 3D high-power processor thermal behavior using novel radial expanding channels and pin fields cooled using two-phase dielectric fluid were constructed in [16]. An effective critical heat flux where the average core temperature rise was less than 30 °C was found to be 350W/cm^2, significantly higher than the values observed for longer parallel channels. Two-phase cooling with ultra-low Global Warming Potential (GWP) dielectric fluids R1233zd(E) and R1234ze(E) was studied in [17]. The results showed that compared to water cooling, two-phase cooling achieves lower junction temperatures and more uniform cooling for the same flow rates and pumping power. Along with direct liquid cooling using cold plate, another approach in liquid cooling is immersion cooling [18-20] where the whole chip is submerged inside dielectric coolants.

As compared to component level, there are fewer number of studies conducted for rack level liquid cooling due to cost and complexity of the equipment. Fluid distribution in a two-phase cooled rack under steady and transient information technology loads was investigated in [21]. The flow rates and pressure distribution across the rack are studied in various filling ratios. A control system was designed to regulate the temperature of the supplied coolant in response to the step change in the IT workload. Alkharabsheh [22] performed a rack level experiment to analyze pressure drop of a liquid cooled rack. It was found that pressure drop in the server module was found to cause the highest pressure drop among the coolant distribution unit module and the manifold module which includes the tubing and fittings. A rack level study of hybrid cooled servers using warm water cooling for distributed vs. centralized pumping systems was performed [23]. They found that centralized pumping system has shown relatively lower operating component temperatures and pumping power compared to distributed pumping system.

Although there are significant number of two-phase cooling studies, more works are required to improve knowledge of two-phase cooling with different coolants, operating parameters and geometry parameters. In the current study, a two-phase cooling study using dielectric coolant Novec/HFE 7000 and an impinging/microchannel cold plate was performed in component level. A copper block heater arrangement was used to mimic a computer chip. Effects of subcooling and flow rate on both thermal and pressure drop through the cold plate were presented in detail. Two sizes of tubing connected to cold plates were tested and the effects of inner diameter of tubing on thermal resistance and pressure drop of cold plate are discussed. The experiment was carried out with a large heated surface of 6.45 cm^2 and maximum dissipated heat flux was around 96.1 w/cm^2 corresponding to chip power of 620 W.

2. EXPERIMENTAL SETUP AND PROCEDURES

2.1 Flow Loop

A schematic diagram of the experimental test loop is shown in Fig. 1. A centrifugal pump drives the dielectric liquid, Novec/HFE 7000, through the closed loop. Table 1 shows typical physical properties of Novec/HFE 7000. A liquid-to-liquid heat exchanger located downstream of the test section condenses the vapor and cools the fluid before it enters the

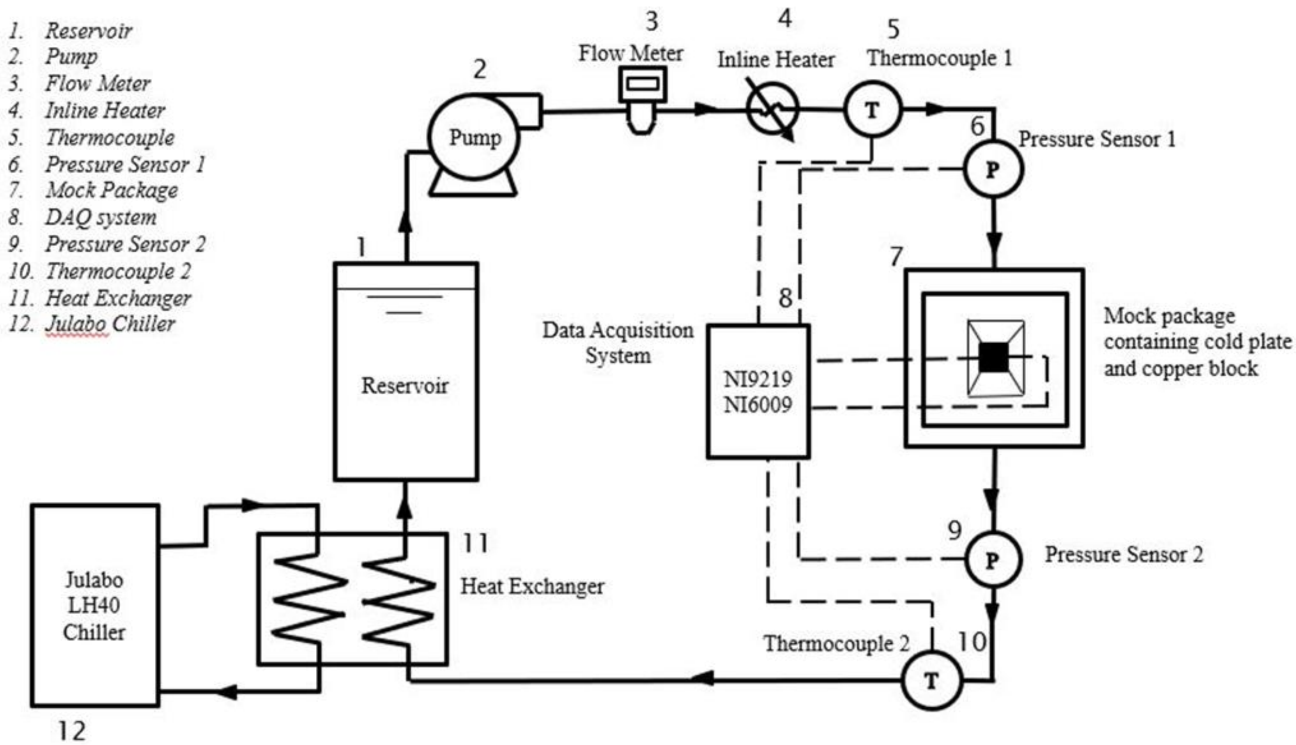

Fig. 1. Schematic illustration of the flow loop.

Table 1. Typical physical properties of Novec/HFE 7000.

Coolant	Molecular Weight (g/mol)	Boiling Point at 1 atm (ºC)	Liquid Density (Kg/m^3)	Kinematic Viscosity (cSt)	Laten Heat of Vaporization (kJ/kg)	Specific Heat (J/KgK)	Surface Tension (dynes/cm)	Thermal Conductivity (W/mK)
HFE 7000	200	34	1400	0.32	142	1300	12.4	0.075

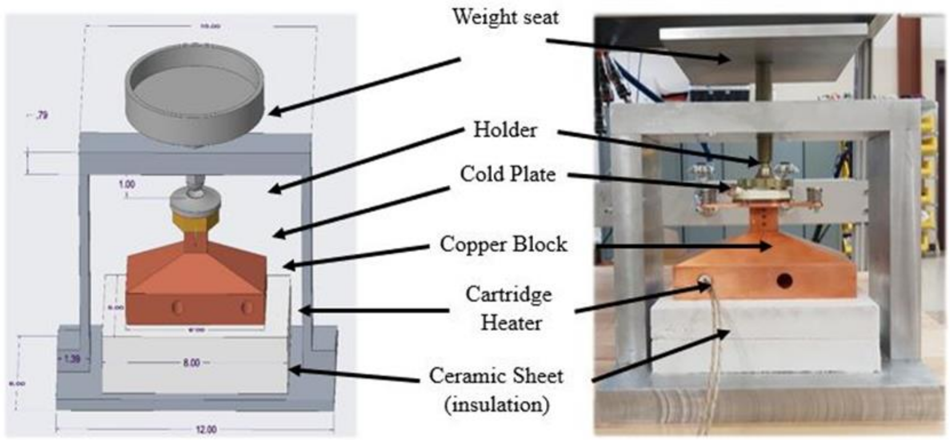

Figure 4. Mock Package

reservoir. This liquid-to-liquid heat exchanger is connected to a chiller (Julabo LH40) for controlling the coolant temperature entering the microchannel heat sink. The liquid is fully degassed before initiating each test using the degassing ports. A flow meter with a measurement range of 0.2–2 l/min monitors the flow rate through the loop and two T-type thermocouples measure the fluid temperature before and after the heat sink. The pressure at the inlet manifold and the pressure drop across the microchannel heat sink are measured using a pressure transducer (Omega, PX309050A5V) and a differential pressure transducer (Omega, PX2300 series), respectively.

2.1 Heat Sink Design and Mock Package

The heat sink shown in Fig. 2a and Fig 2.b consists of a copper microchannel heat sink and manifold. The coolant impinges down the base through a trapezoidal groove at the middle of the heat sink. After impinging down to the base, coolant spread to the sides and go along microchannels. This structure of heat sink assures that coolant can has high surface contact area with copper microchannels and enhance both forced convection and boiling. Mock package is shown in Fig. 4. The copper block with 4 cartridge heaters is placed on top of a ceramic fiber sheet. Each cartridge heater can deliver power up to 400 W. There were three J-type thermocouples installed to copper block for measuring heat flux using Fourier's law. Cold plate is placed on top surface of copper block with thermal interface material in between. The cold plate was fixed onto the top-surface of copper block by a holder of the frame. Weights were placed on the weight seat for maintaining pressure and constant interfacial thickness. Details of mock package design and the components of mock package are available in Hoang et al. [24].

Two slots with a width of 0.03" and 0.03" deep was cut to accommodate T-type thermocouples as shown in the figure 3 in order to measure the heat sink's base metal temperature T_b. A very tight machining tolerance was maintained while making the slots. Heat sink thermal resistance R_{th} is represented by ratio of difference between average base temperature T_b and incoming coolant T_{in} to input power supplied or heat picked by the coolant $\dot{Q}$. Two T-type thermocouples fabricated at the facility were calibrated using a precision oven before setting them on the grooves.

Figure 2a. Cold plate manifold and fin part

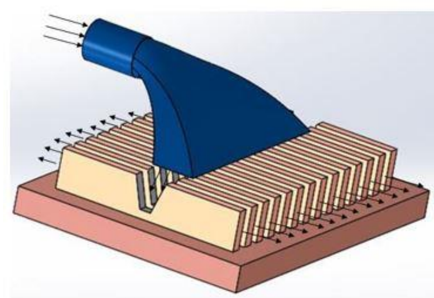

Figure 2b. Schema of the cold plate design

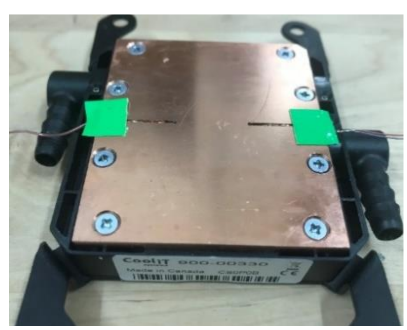

Figure 3. T-type thermocouples installed in the back of the cold plate to indicate base temperature measurement T_b during thermal tests.

2.2 Experimental Procedures

Three mass flux values ranging from 547 to 958 kg/m^{2}s are investigated to map the effect of flow velocity on boiling. Before initiating each test, the liquid in the test loop is fully degassed to help reduce flow instabilities. The inlet coolant temperature is controlled by adjusting temperature of secondary loop via the Julabo LH40 chiller. A constant flow rate was maintained by adjusting the supplied DC power to the centrifugal pump. The coolant flow rate is controlled in order to ensure that a constant flow rate is maintained throughout the experiments. Coolant enters inlet of heat sink in single-phase and leaves heat sink as a two-phase mixture of liquid and vapor. After leaving the heat sink, the mixture of vapor and liquid was condensed to single-phase liquid inside the liquid-liquid heat exchanger which is connected to a Julabo LH40 chiller. The single-phase liquid after leaving the heat exchanger was returned to the reservoir and finish the cycle.

3. Heat Loss and Uncertainty Analysis

Several tests are performed in a single-phase state to determine the heat losses via measuring the difference between sensible heat absorbed by the coolant and the measured electrical power input. The heat loss in single-phase regime is calculated by: $Q_{loss} = Q_{electric} - m' C\Delta T$. Where Qelectric is electrical input power from the cartridge heater, m is mass flow rate (kg/s), C is specific heat (J/kg.^{o}C) and ΔT (^{o}C) is temperature difference between outlet and inlet of heat sink. Heat of evaporation is not mentioned in this equation because in order to calculate heat loss, experiment was operated in single-phase regime with heat flux lower than onset of nucleate boiling point. $Q_{coolant}$ in the Figure 5. was sensible heat absorbed by the coolant and can be evaluated by $Q_{coolant} = m' C\Delta T$. Q_{loss} was less than 5 % in all data points.

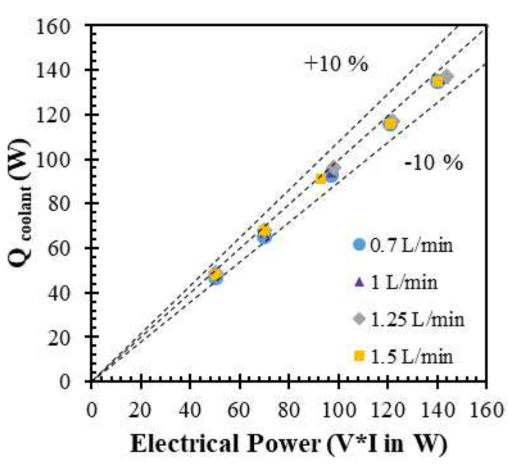

Figure 5. Energy balance comparison between electrical power and heat absorbed by coolant at different flow rates

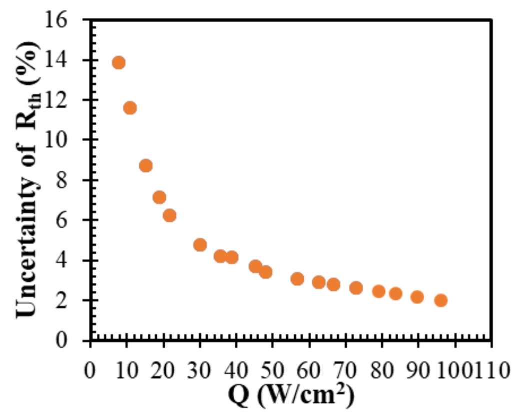

Figure 6. Experimental uncertainty of thermal resistance for various heat fluxes.

The uncertainties in measurement of sensors are shown in table 2. The uncertainty of thermal resistance was calculated using root sum square method [24, 25, 28] and reduced with heat flux from 13 % at heat flux 7 W/cm^2 to 2 % at heat flux 96 W/cm^2. Variation of uncertainty in measurement of thermal resistance was presented in Figure 6. Uncertainty in measurement of pressure drop was 3.8 %.

4. Results and Discussion

4.1 Subcooling Effects

Experiments were conducted at three subcooling levels: 5 degree subcooling, 10 degree subcooling and 15 degree subcooling. The saturation pressure is 22.5 psi corresponding to saturation temperature 51 ^{o}C. It can be observed in Fig 7. that thermal resistance increases with subcooling. Specific thermal resistance was calculated by the formula:

$$R_{th} = \frac{A(T_b - T_{in})}{Q}$$

Where T_b is the base temperature at the bottom of the heat sink, T_{in} is the inlet temperature of the coolant, Q is the total heat absorbed by the heat sink and coolant and A is the area covered by the microchannels of heat sink. When experiment was operated at lower subcooling, more latent heat was utilized to remove heat flux, and this resulted in highest thermal performance for lower subcooling case. Although having lowest thermal resistance, it can be seen in Fig. 8 that the case of 5 degree subcooling has highest base temperature. The higher base temperature in case of lower subcooling is attributed to the increase of inlet temperature when subcooling is reduced. The base temperature did not exceed 61 ^{o}C at maximum heat flux of 69 W/cm^2 in the case of 5 degree subcooling and inlet temperature of 48 ^{o}C.

Table 2. Instruments and uncertainties

Instruments	Measurand	Uncertainty	DAQ Module
Pressure Gauges (Omega): PX309050A5V	P_{in}, P_{out}	±0.8 kPa	NI- USB-6009
T-type Thermocouple: Laboratory Made	T_{in}, T_{out}, T_b	± 0.2°C	NI 9219
Thermocouple (Omega): TJ36-CASS-116E-2-CC	Heat Flux Measurement	± 0.2°C	NI 9219

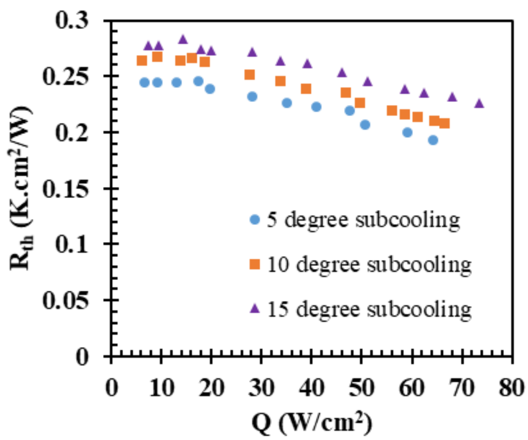

Figure 7. Effects of subcooling on thermal resistance

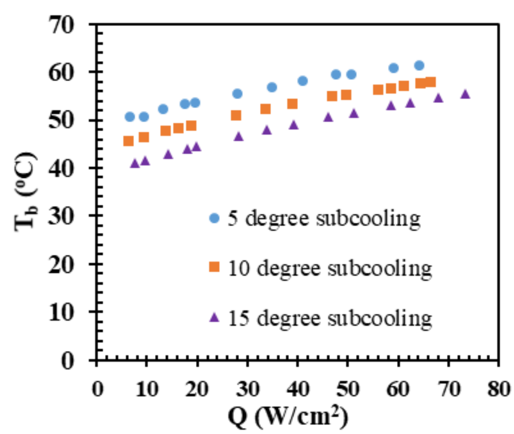

Figure 8. Effects of subcooling on base temperature of heat sink

Effects of subcooling on pressure drop was presented in Fig. 9. Pressure drop was observed to increase with subcooling in single-phase regime due to the increase of viscosity with reducing of coolant inlet temperature. In two-phase regime, the trend reverses, pressure drop reduces with subcooling because lower amount of vapor bubbles were created at higher subcooling [26]. Pressure drop in single-phase regime was from 9 to 10 Kpa and pressure drop in two-phase regime increases significantly with heat flux and reaches the maximum value of 18.8 Kpa for the case of 5 degree subcooling. These pressure drop values for both single-phase and two-phase regimes are well below critical pressure drop through each heat sink. When liquid-cooling heat sinks are connected in series in data center cooling rack system, the pressure drop through three heat sinks in series should not exceed 10 psi (or 68.95 Kpa).

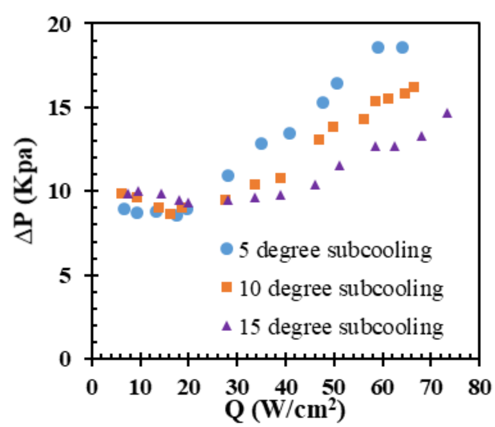

Figure 9. Effects of subcooling on pressure drop through heat sink

4.2 *Effects of flow rate*

Effects of flow rate on thermal resistance was presented in Figure 10. At lower heat fluxes, thermal resistance did not vary significantly with heat flux due to single-phase heat transfer mechanism. When heat flux was increased further, vapor started to occur, and thermal resistance decreased with heat flux. At lower heat fluxes and single-phase regime, thermal resistance is highly dependent on flow rate. Thermal resistance in single-phase regime for flow rate 0.7 L/min was around 0.44 K.cm^2/W and thermal resistance in single-phase regime for flow rate 1.75 L/min was 0.24 K.cm^2/W. At higher heat fluxes, it was observed that thermal resistance was weakly dependent on flow rate due to nucleate boiling two-phase heat transfer mechanism. Thermal resistance at the same heat flux of 72 W/cm^2 was 0.26 K.cm^2/W for flow rate 0.7 L/min and 0.19 K.cm^2/W for flow rate 1.5 L/min.

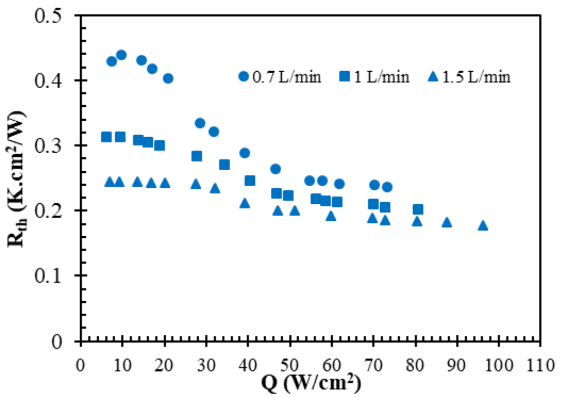

Figure 10. Effects of flow rate on the thermal resistance of the heat sink

Effects of flow rate on pressure drop was presented in Figure 11. It was observed that the onset of nucleate boiling point was delayed when flow rate was increased from 0.7 L/min to 1.5 L/min. The onset of nucleate boiling for flow rate 0.7 happened at heat flux 18 W/cm^2, while the onset of nucleate boiling in the case of flow rate 1.5 L/min occurred at heat flux 41 W/cm^2. Pressure drop generally does not change much in single-phase regime but increases significantly when vapor started to occur at onset of nuclear boiling point. The increasing of pressure drop in two-phase regime is attributed to acceleration and friction factors caused by vapor. The pressure drops for flow rates 0.7 L/min, 1 L/min and 1.5 L/min at the same heat flux 75 W/cm^2 were 16 Kpa, 16.5 Kpa and 21 Kpa respectively. It is beneficial to reduce flow rate for lower pressure drop or pumping power; however, engineers and scientists should be aware of lower critical heat flux at lower flow rate. It should be noticed that in two-phase regime there is not significant difference in pressure drop between flow rate 0.7 L/min and 1 L/min. When flow rate is increased, vapor production decreases and lead to reduction of pressure drop of vapor fraction. However, pressure drop due to acceleration and friction increased with higher flow rate. The decrease of pressure drop due to lower vapor production and the increase of pressure drop due to higher flow rate almost cancel each other; therefore, no significant difference in pressure drop was observed between flow rate 0.7 L/min and 1 L/min. However, when flow rate increases to considerably higher value of 1.5 L/min, the increase of pressure drop due to acceleration factor surpassed the decrease of pressure drop due to lower vapor production. As a result, pressure drop at flow rate 1.5 L/min increased to 21 Kpa and was much higher than pressure drop at flow rate 0.7 and 1 L/min.

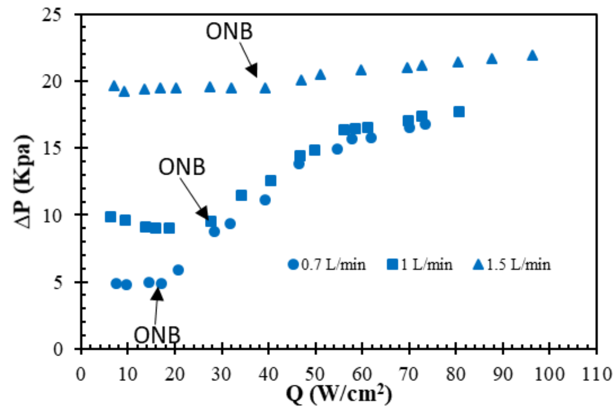

Figure 11. Effects of flow rate on the pressure drop through the heat sink, T_{in} = 36 °C, T_{sat} = 54 °C

The Figure 12 presented boiling curve as a function of flow rate for the heat sink at coolant inlet temperature 36 °C and saturation temperature 51 °C. The variation of wall super heat $\Delta T = T_w - T_{sat}$ with heat flux was presented in Figure 12. For convective flows in tubes and channels, the onset of nucleate boiling (ONB) marks the beginning of the transition from single-phase liquid convection to combined convection and nucleate boiling. In a convective flow of this type, the onset is usually defined as occurring at the location where active nucleation sites are first observed [27]. The wall super heat ΔT increases linearly with heat flux and boiling did not occur until heat flux equals to 18 W/cm^2 for flow rate 0.7 L/min. As the wall temperature increases, the subcooled nucleate boiling contribution generally becomes large compared to the single-phase liquid convection contribution. In nucleate boiling, the heat transfer performance is not highly dependent on flow rate like in single-phase regime and wall super heat ΔT in three flow rates 0.7, 1 and 1.5 L/min seem to have the similar values. At the same heat flux of 78 W/cm^2, wall super heat has value of 10.1, 9.9 and 9.5 °C for flow rate 0.7 L/min, 1 L/min and 1.5 L/min, respectively.

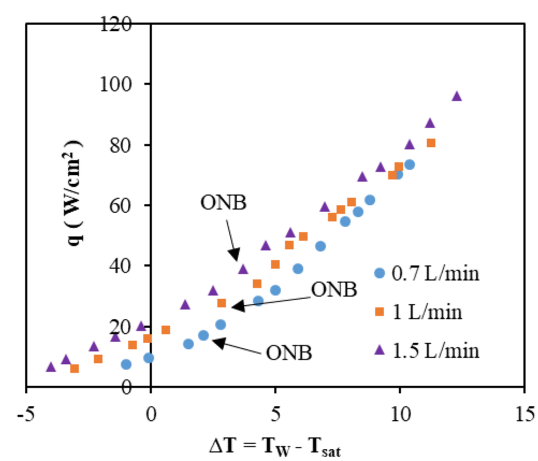

Figure 12. Boiling curves as a function of volumetric flow rate for the heat sink, T_{in} = 36 °C, T_{sat} = 54 °C

4.3 Effects of Tubing Sizes

Two tubing sizes with inner diameters of 5/32 inch and 1/4 inch were studied in current research. Figure 13 shows thermal resistance at flow rates 0.7 L/min and 1 L/min for the case of tubing 5/32 inch and 1/4 inch. It is observed that in two-phase regime, thermal resistance in the case of tubing 1/4 inch was much lower than thermal resistance in the case of tubing 5/32 inch. At flow rate 1 L/min, thermal resistance in the case of tubing 1/4 inch was 0.21 K.cm^2/W as compared to thermal resistance of 0.31 K.cm^2/W in the case of tubing 5/32 inch. In the case of bigger tubing size, lower pressure at the outlet leads to lower boiling point and higher vapor quality and higher amount of heat flux was removed by latent heat. Therefore, thermal performance in the case of tubing size 1/4 inch was improved as compared to tubing size 5/32 inch. Figure 14 presented pressure drop at flow rates 0.7 L/min and 1 L/min for the case of tubing 5/32 inch and 1/4 inch. At the same heat flux 80 W/cm^2 and flow rate 1 L/min, pressure drop in the case of tubing 1/4 inch was 17 Kpa; meanwhile pressure drop in the case tubing 5/32 inch was 47 Kpa.

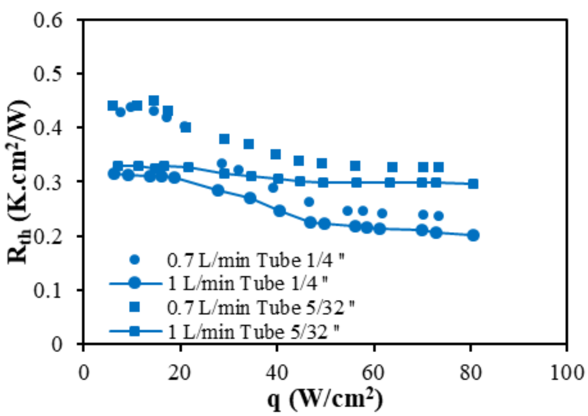

Figure 13. Effects of tubing size on the thermal performance of heat sink

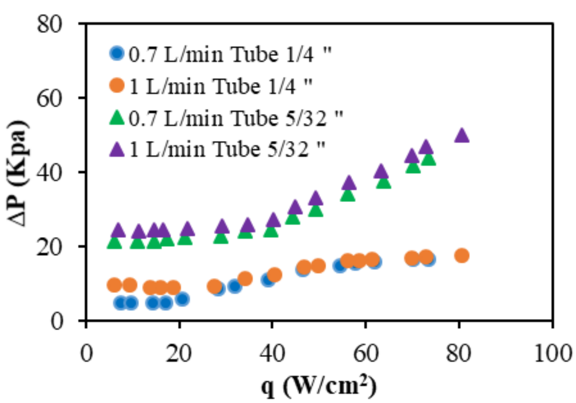

Figure 14. Effects of tubing size on the pressure drop through the heat sink

Conclusion

In this study, we investigate the thermal and hydraulic performance of a microchannel/impingement two-phase heat sink vs flow rate, subcooling and tubing size with dielectric coolant Novec/HFE-7000. The main findings from this study are given as follows:

- Lower subcooling leads to lower thermal resistance. Although having lower thermal resistance, lower subcooling can result in higher base temperature. The higher base temperature in case of lower subcooling is attributed to the increase of inlet temperature when subcooling is reduced. Pressure drop increases with subcooling in single-phase regime but decreases with subcooling in two-phase regime.
- Thermal resistance is independent on heat fluxes and highly dependent on flow rate at lower heat fluxes and single-phase regime. On the other hand, in two-phase regime (nucleate boiling), thermal resistance is weakly dependent on flow rate and decreases with heat flux. Pressure drop generally increases with flow rate and heat fluxes in two-phase regime.
- An increase of tubing size from 5/32 inch to 1/4 inch results in 47 % decrease in thermal resistance and 63 % decrease in pressure drop. The decrease of pressure at the outlet of heat sink due to bigger tubing size lead to higher vapor quality and improvement in thermal performance.

ACKNOWLEDGEMENT

The research reported herein was supported by a grant from the National Science Foundation Industry/University Cooperative Research Center Award No. IIP-1738793 and the Semiconductor Research Corporation (SRC). The author would like to thank Mr. Eugene Mazza from Mechanical Specialties at Binghamton, NY for his help towards machining the cold plate.

REFERENCE

1. N. Jones, "How to stop data centres from gobbling up the world's electricity," *Nature*, vol. 561, no. 7722, pp. 163–166, 2018, doi: 10.1038/d41586-018-06610-y.
2. S. V. Garimella, T. Persoons, J. Weibel, and L. T. Yeh, "Technological drivers in data centers and telecom systems: Multiscale thermal, electrical, and energy management," *Appl. Energy*, vol. 107, pp. 66–80, 2013, doi: 10.1016/j.apenergy.2013.02.047.
3. Arman Shehabi, S. Smith, Dale A Sartor, R. Brown, M. Herrlin, J. Koomey, E. Masanet, N. Horner, I. Azevedo, W. Lintner, "United States Data Center Energy Usage Report | Energy Technologies Area," no. June, p. 65, 2016, [Online]. Available: https://eta.lbl.gov/publications/united-states-data-center-energy.
4. R. Schmidt, "Packaging of New Servers, Energy Efficiency Aspects," *1st Berkeley Symposium on Energy Efficient Electronics.*, Aug. 9-12, 2009.
5. Gao, Tianyi, Shuai Shao, Yan Cui, Bryan Espiritu, Charles Ingalz, Hu Tang, and Ali Heydari. 2017. "A Study of Direct Liquid Cooling for High-Density Chips

and Accelerators.” *Proceedings of the 16th InterSociety Conference on Thermal and Thermomechanical Phenomena in Electronic Systems, ITherm 2017*, 565–73. https://doi.org/10.1109/ITHERM.2017.7992537.

6. Nadjahi, Chayan, Hasna Louahlia, and Stéphane Lemasson. 2018. “A Review of Thermal Management and Innovative Cooling Strategies for Data Center.” *Sustainable Computing: Informatics and Systems* 19 (May): 14–28. https://doi.org/10.1016/j.suscom.2018.05.002.
7. Zhang, Kai, Yiwen Zhang, Jinxiang Liu, and Xiaofeng Niu. 2018. “Recent Advancements on Thermal Management and Evaluation for Data Centers.” *Applied Thermal Engineering* 142 (April): 215–31. https://doi.org/10.1016/j.applthermaleng.2018.07.004.
8. Z. Deng, J. Shen, W. Dai, Y. Liu, Q. Song, W. Gong, K. Li, M. Gong “Flow and thermal analysis of hybrid mini-channel and slot jet array heat sink,” *Appl. Therm. Eng.*, vol. 171, 2020, doi: 10.1016/j.applthermaleng.2020.115063.
9. Y. Hadad, N. Fallahtafti, L. Choobineh, C. H. Hoang, V. Radmard, P. Chiarot , B. Sammakia, "Performance Analysis and Shape Optimization of an Impingement Microchannel Cold Plate," in *IEEE Transactions on Components, Packaging and Manufacturing Technology*, vol. 10, no. 8, pp. 1304-1319, Aug. 2020, doi: 10.1109/TCPMT.2020.3005824.
10. Hoang, CH, Tradat, M, Manaserh, Y, Ramakrisnan, B, Rangarajan, S, Hadad, Y, Schiffres, S, & Sammakia, B. "Liquid Cooling Utilizing a Hybrid Microchannel/Multi-Jet Heat Sink: A Component Level Study of Commercial Product." *Proceedings of the ASME 2020 International Technical Conference and Exhibition on Packaging and Integration of Electronic and Photonic Microsystems*. *ASME 2020 International Technical Conference and Exhibition on Packaging and Integration of Electronic and Photonic Microsystems*. Virtual, Online. October 27–29, 2020. V001T08A008. ASME. https://doi.org/10.1115/IPACK2020-2627
11. A. C. Kheirabadi and D. Groulx, “Cooling of server electronics: A design review of existing technology,” *Appl. Therm. Eng.*, vol. 105, no. 2016, pp. 622–638, 2016, doi: 10.1016/j.applthermaleng.2016.03.056.
12. B. Rimbault, C. T. Nguyen, and N. Galanis, “Experimental investigation of CuO-water nanofluid flow and heat transfer inside a microchannel heat sink,” *Int. J. Therm. Sci.*, vol. 84, pp. 275–292, 2014, doi: 10.1016/j.ijthermalsci.2014.05.025.
13. Ohadi, M M, S V Dessiatoun, K Choo, M Pecht, and J V Lawler. 2012. “A Comparison Analysis of Air, Liquid, and Two-Phase Cooling of Data Centers.” In *2012 28th Annual IEEE Semiconductor Thermal Measurement and Management Symposium (SEMI-THERM)*, 58–63. https://doi.org/10.1109/STHERM.2012.6188826.
14. K. W. Jung, C. Kharangate, H. Lee, J. W. Palko “Microchannel cooling strategies for high heat flux (1 kW/cm2) power electronic applications,” in *2017 16th IEEE Intersociety Conference on Thermal and Thermomechanical Phenomena in Electronic Systems (ITherm)*, 2017, pp. 98–104, doi: 10.1109/ITHERM.2017.7992457.
15. Ren, Q, H Yu, Y Liu, and Z Wang. 2020. “The Investigation of the Silicon Fabricated Balanced Shunt Micro Pin Fins Cold Plate for High Heat Flux Devices.” In *2020 19th IEEE Intersociety Conference on Thermal and Thermomechanical Phenomena in Electronic Systems (ITherm)*, 950–56. https://doi.org/10.1109/ITherm45881.2020.9190295.
16. M. Schultz, F. Yang, E. G. Colgan, R. Polastre, B. Dang, C. Tsang, M. A. Gaynes, “Embedded two-phase cooling of large three-dimensional compatible chips with radial channels,” *J. Electron. Packag. Trans. ASME*, vol. 138, no. 2, pp. 1–5, 2016, doi: 10.1115/1.4033309.
17. Karwa, N. 2020. “Ultra-Low Global Warming Potential Heat Transfer Fluids for Pumped Two-Phase Cooling in HPC Data Centers.” In *2020 19th IEEE Intersociety Conference on Thermal and Thermomechanical Phenomena in Electronic Systems (ITherm)*, 283–90. https://doi.org/10.1109/ITherm45881.2020.9190269.
18. D. K. Harris, J. Gess, S. Bhavnani, B. Ramakrisnan, R. W. Johnson, R. W. Knight, M. Hamilton, C. Ellis, “Impact of surface enhancements upon boiling heat transfer in a liquid immersion cooled high performance small form factor server model,” in *Fourteenth Intersociety Conference on Thermal and Thermomechanical Phenomena in Electronic Systems (ITherm)*, 2014, pp. 435–443, doi: 10.1109/ITHERM.2014.6892314.
19. M. Wada, A. Matsunaga, M. Hachiya, M. Chiba, K. Ishihara, and M. Yoshikawa, “Feasibility study of two-phase immersion cooling in closed electronic device,” in *2017 16th IEEE Intersociety Conference on Thermal and Thermomechanical Phenomena in Electronic Systems (ITherm)*, 2017, pp. 899–904, doi: 10.1109/ITHERM.2017.7992581.
20. J. M. Shah, C. Bhatt, P. Rachamreddy, R. Dandamudi, S. Saini, and D. Agonafer, “Computational Form Factor Study of a 3rd Generation Open Compute Server for Single-Phase Immersion Cooling.” Oct. 07, 2019, doi: 10.1115/IPACK2019-6602.
21. S. Khalili, S. Rangarajan, V. Gektin, H. Alissa, and B. Sammakia, “An Experimental Investigation on the Fluid Distribution in a Two-Phase Cooled Rack Under Steady and Transient Information Technology Loads,” *J. Electron. Packag.*, vol. 142, no. 4, Sep. 2020, doi: 10.1115/1.4048180.
22. S. Alkharabsheh, B. Ramakrishnan, and B. Sammakia, “Pressure drop analysis of direct liquid cooled (DLC) rack,” in *2017 16th IEEE Intersociety Conference on Thermal and Thermomechanical Phenomena in Electronic Systems (ITherm)*, 2017, pp. 815–823, doi: 10.1109/ITHERM.2017.7992570.
23. M. Sahini, J. E. Fernandes, V. Mulay, P. Mcginn, D. Agonafer, “Rack-level study of hybrid cooled servers using warm water cooling for distributed vs. centralized pumping systems,” in *2017 33rd Thermal Measurement, Modeling & Management Symposium (SEMI-THERM)*, 2017, pp. 155–162, doi: 10.1109/SEMI-THERM.2017.7896924.

24. C. H. Hoang, S. Khalili, B. Ramakrisnan, S. Rangarajan, Y. Hadad, V. Radmard, K. Sikka, S. Schiffres, B. Sammakia, “An Experimental Apparatus for Two-phase Cooling of High Heat Flux Application using an Impinging Cold Plate and Dielectric Coolant,” in *2020 36th Semiconductor Thermal Measurement, Modeling & Management Symposium (SEMI-THERM)*, 2020, pp. 32–38, doi: 10.23919/SEMI-THERM50369.2020.9142831.
25. R. J. Moffat, “Describing the uncertainties in experimental results,” *Exp. Therm. Fluid Sci.*, vol. 1, no. 1, pp. 3–17, 1988, doi: https://doi.org/10.1016/0894-1777(88)90043-X.
26. C. H. Hoang, S. Rangarajan, S. Khalili, B. Ramakrisnan, V. Radmard, Y. Hadad, S. Schiffres, B. Sammakia, “Hybrid microchannel/multi-jet two-phase heat sink: A benchmark and geometry optimization study of commercial product,” *Int. J. Heat Mass Transf.*, vol. 169, p. 120920, 2021, doi: https://doi.org/10.1016/j.ijheatmasstransfer.2021.120920.
27. V.P. Carey, Liquid-vapor phase-change phenomena : an introduction to the thermophysics ofvaporization and condensation processes in heat transfer equipment, 2nd ed., New York : Taylor and Francis, 2008. http://lib.ugent.be/catalog/rug01:001430011.
28. B. Ramakrishnan, C. H. Hoang, S. Khalili, Y. Hadad, S. Rangarajan, A. Pattamatta, B. Sammakia, “Experimental Characterization of Two-Phase Cold Plates Intended for High-Density Data Center Servers Using a Dielectric Fluid,” *J. Electron. Packag.*, vol. 143, no. 2, Mar. 2021, doi: 10.1115/1.4049928.